HYDROLOGICAL PROCESSES
Hydrol. Process. (in press)
Published online in Wiley InterScience (www.interscience.wiley.com). DOI: 10.1002/hyp.1187

Wavelet analysis of inter-annual variability in the runoff regimes of glacial and nival stream catchments, Bow Lake, Alberta

Melissa Lafrenière* and Martin Sharp
Department of Earth and Atmospheric Science, 1–16 Earth Sciences Building, University of Alberta, Edmonton, AB T6G 2R3, Canada

Abstract:

Continuous wavelet analyses of hourly time series of air temperature, stream discharge, and precipitation are used to compare the seasonal and inter-annual variability in hydrological regimes of the two principal streams feeding Bow Lake, Banff National Park, Alberta: the glacial stream draining the Wapta Icefields, and the snowmelt-fed Bow River. The goal is to understand how water sources and flow routing differ between the two catchments. Wavelet spectra and cross-wavelet spectra were determined for air temperature and discharge from the two streams for summers (June–September) 1997–2000, and for rainfall and discharge for the summers of 1999 and 2000. The diurnal signal of the glacial runoff was orders of magnitude higher in 1998 than in other years, indicating that significant ice exposure and the development of channelized glacial drainage occurred as a result of the 1997–98 El Niño conditions. Early retreat of the snowpack in 1997 and 1998 led to a significant summer-long input of melt runoff from a small area of ice cover in the Bow River catchment; but such inputs were not apparent in 1999 and 2000, when snow cover was more extensive. Rainfall had a stronger influence on runoff and followed quicker flow paths in the Bow River catchment than in the glacial catchment. Snowpack thickness and catchment size were the primary controls on the phase relationship between temperature and discharge at diurnal time scales. Wavelet analysis is a fast and effective means to characterize runoff, temperature, and precipitation regimes and their interrelationships and inter-annual variability. The technique is effective at identifying inter-annual and seasonal changes in the relative contributions of different water sources to runoff, and changes in the time required for routing of diurnal meltwater pulses through a catchment. However, it is less effective at identifying changes/differences in the type of the flow routing (e.g. overland flow versus through flow) between or within catchments. Copyright © 2003 John Wiley & Sons, Ltd.

KEY WORDS wavelets; snow and glacier hydrology; Bow Lake; air temperature–runoff relationships

INTRODUCTION

Runoff from alpine catchments is typically dominated by snow and ice melt, which peak in spring and summer. Intra- and inter-annual variability in runoff regimes result from variations in winter snowfall and summer meteorological conditions. In some areas, variability at both time scales may be strongly coupled to atmospheric teleconnection patterns such as the El Niño–southern oscillation (ENSO), the Pacific decadal oscillation (PDO), and the North Atlantic oscillation (NAO) (Redmond and Koch, 1991; Kahya and Dracup, 1993; Dracup and Kahya, 1994; Brown, 1998; Moore and Demuth, 2001). Inter-catchment differences in runoff regimes may reflect differences in the dominant runoff sources (snow, glacier ice, and rainfall) and in the flow routing within the catchments. These influences also affect processes such as acidification (Stoddard, 1995), nutrient and carbon budgets (Brooks *et al*., 1995; Boyer *et al*., 1997), and the transport of organic (Blais *et al*., 2001a,b) and inorganic contaminants.

* Correspondence to: Melissa Lafrenière, Department of Earth and Atmospheric Science, 1–16 Earth Sciences Building, University of Alberta, Edmonton, AB T6G 2R3, Canada. E-mail: melissa.lafreniere@ualberta.ca

Received 11 October 2001
Accepted 10 June 2002

This paper investigates the runoff regimes of two adjacent alpine catchments (one largely glacier covered and one virtually ice free), their relationship to meteorological forcing, and their inter-annual variability over an ENSO cycle. Wavelet analyses of temperature, discharge, and rainfall time series are used to compare the seasonal and inter-annual variability of hydrological processes operating in the two catchments in four consecutive summers (1997–2000). As this period includes the strong 1998 El Niño event, the meteorological and discharge time series data provide a unique opportunity to examine the hydrological regimes of the glacial and non-glacial streams under contrasting hydroclimatological conditions.

In snow- and ice-covered catchments, solar radiation is the primary force driving the seasonal hydrological cycle. Although net radiation is the main energy source for melt, air temperature is usually better correlated with melt production and run-off than net radiation (Braithwaite, 1981). Therefore, air temperature is used here as a proxy for melt energy input to the catchments. As the melt season progresses, the relationship between discharge and air temperature evolves. This is due to changes in snowpack extent, the exposure of glacial ice, and the storage of meltwater in the snowpack, glacier (i.e. due to development of englacial and subglacial drainage systems), and/or shallow soils and groundwater. Thus, the relationship between temperature and runoff contains information about the transfer and storage processes operating in the catchment.

Many recent studies have applied a combination of time domain statistical techniques to climatic and hydrological time series data from glacial catchments to infer changes in the functioning of glacier drainage systems during the ablation season (Gurnell *et al*., 1992; Hodgkins, 2001). These techniques include linear regression, cross-correlation, autoregressive integrated moving average (ARIMA) and transfer function-noise (TFN) models. Other studies have used spectral (Fourier transform) analysis to investigate the relationships between meteorological conditions and runoff in glacial catchments (Gudmundsson, 1970; Gudmundsson and Sigbjarnarson, 1972). This paper presents the first application of the continuous wavelet transform to the analysis of air temperature–runoff relationships. Wavelet analysis is a time-dependent spectral analysis that decomposes a data series in time–frequency space. Wavelet methods have been used for more than a decade in many different types of signal and image analysis (Kadambe and Boudreaux-Bartels, 1992; Kronland-Martinet *et al*., 1987; Schiff, 1992). Recently, the use of wavelets has expanded into the physical Earth sciences (Whitfield and Dohan, 1997; Smith *et al*., 1998; Torrence and Compo, 1998; Labat *et al*., 2000).

The lack of a static 24 h discharge cycle, and the dynamic nature of the temperature–runoff relationship make continuous quantitative analysis of the amplitude and the timing of runoff response to air temperature inputs difficult using standard time series techniques. For example, regression and cross-correlation techniques require several steps of data preparation, and the subdivision of the time series into periods of similar behaviour to evaluate seasonal changes in the time series (Gurnell *et al*., 1992; Hodgkins, 2001). Wavelet methods are better suited to this type of problem, because one can quantify the variability of a series continuously in time and at different scales of response. The covariance (or coherence) and the phase (or lag) relationships of paired time series can also be quantified continuously across both scale and time, by combining the wavelet transforms of the two data sets. The introduction of statistical significance tests by Torrence and Compo (1998) has greatly improved the quantitative nature of wavelet analysis. In this paper, wavelet spectra are determined for air temperature and discharge of the two streams for four consecutive summer seasons (June–September, 1997–2000). The cross-wavelet spectra between air temperature and the two stream runoff series for each year are also determined. Wavelet spectra of rainfall and rain-runoff cross-spectra are calculated for 1999 and 2000.

FIELD SITE AND DATA

Stream discharge and meteorological data were collected at Bow Lake, Banff National Park, Alberta, Canada (51°40′N, 116°27′W) between June 1997 and September 2000. Two main catchments feed Bow Lake: one is largely glacier covered, the other is virtually ice free (<1·5% glacier ice) (Figure 1). The principal inflow to the lake is the 'Glacial' stream (GL) fed primarily by meltwater from the Wapta Icefield. The catchment of

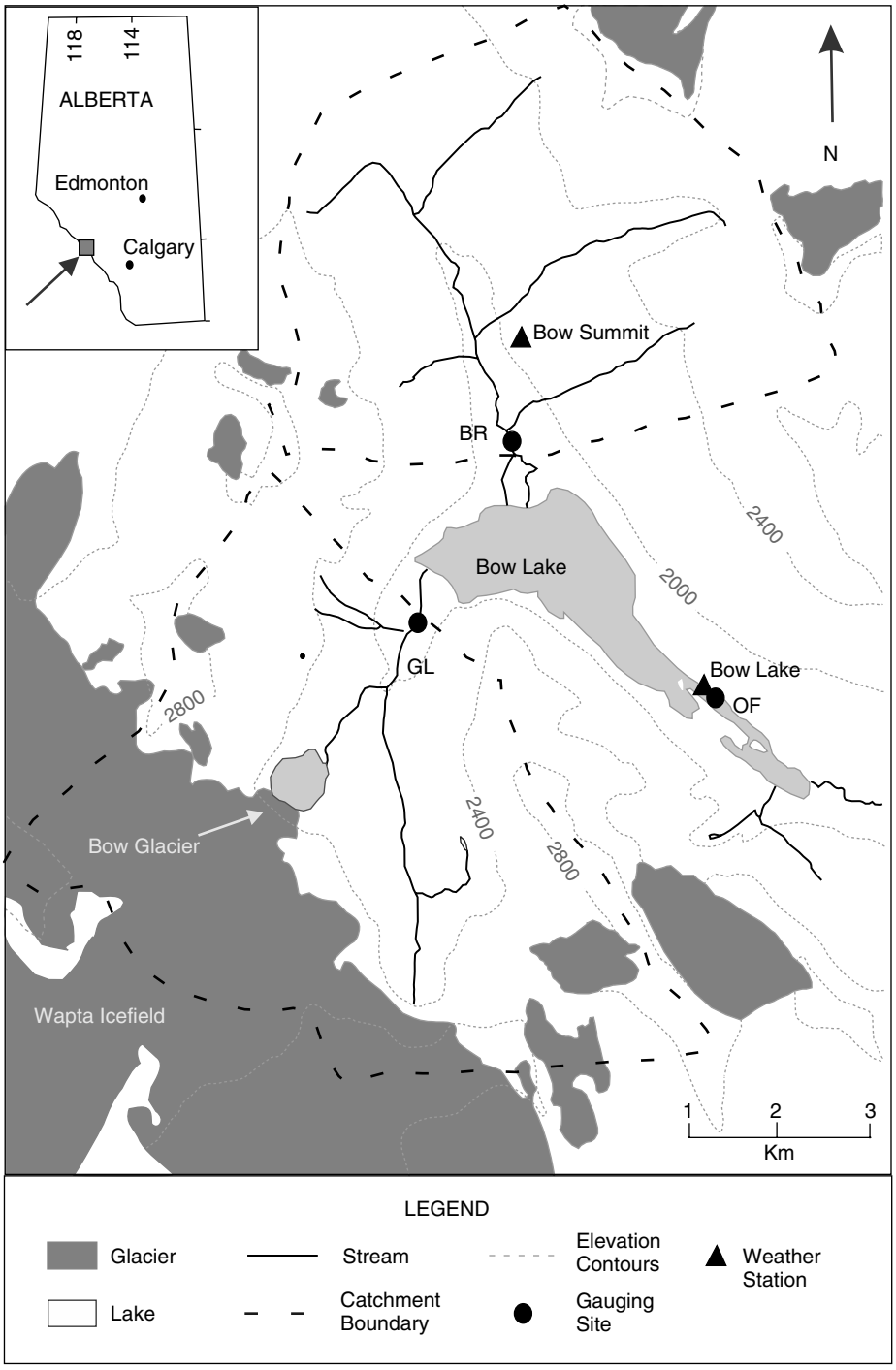

Figure 1. Map of Bow Lake. GL and BR mark the gauging stations for the glacial stream and the Bow River. The Bow Lake meteorological station is located near the outflow gauging station (OF). The location of the Alberta Environment weather station at Bow Summit is also shown

this stream is approximately 27 km^2, has a mean elevation of 2560 m a.s.l., and consists of glacier ice (41%, 11 km^2), till, moraines, and some spruce-fir forest (12%). The secondary inflow is the headwaters of the Bow River (BR). This stream drains into the north side of Bow Lake, and its catchment has a mean elevation of 2310 m a.s.l., 67% of the ~17 km^2 catchment consists of subalpine meadow and spruce-fir forests, but the remaining area is either sparsely vegetated or unvegetated.

Gauging stations were installed in the spring, and removed in the fall of each year. Each gauging station was equipped with a pressure transducer (Keller Series 169). Water pressure was sampled at 10 s intervals and hourly and daily averages were recorded using a Campbell CR10 datalogger. The pressure record was converted to a discharge hydrograph using rating curves. Discharge was measured by the velocity–area method, and at least ten discharge measurements were used to fit the rating curve function. The error associated with the discharge is estimated to be ±10% (Dingman, 1993). Air temperature and rainfall were measured at a meteorological station near the outflow of the lake (Figure 1). Air temperature, measured using a Campbell Scientific Model 107 probe with radiation shield, was sampled every 10 s and averaged hourly and daily. Hourly and daily rainfall totals were measured using a tipping bucket rain gauge (Texas Electronics model TE525). Snowpack accumulation and melt were recorded using an ultrasonic depth gauge (Campbell Scientific model UDG 01).

Difficulties with the power source at the weather station in the summers of 1997 and 1998 resulted in gaps in the temperature and precipitation records. A total of 17 days of data were lost in 1997 (days 222–232, 234–236, and 239–247) and a total of 42 days of data were lost in 1998 (days 167–178, 201–209, 221–232, 235–247). The missing data were interpolated using linear regression equations obtained by establishing a relationship between the Bow Lake data (1940 m a.s.l., 51°39′N, 116°27′E) and data from a station (operated by Alberta Environment) located less than 5 km away, at Bow Summit (2080 m a.s.l., 51°42′N 116°28′E) (Figure 1). Hourly and daily mean values were predicted for temperature. Only daily totals were predicted for precipitation, since the hourly records from the two sites were poorly correlated. For the hourly mean temperature, regressions were calculated using all available points for months where data were missing. For daily mean temperature and total precipitation, regressions were calculated using all the points from June to August ($0{\cdot}80 < r^2 < 0{\cdot}95$). All regressions were significant at $p = 0{\cdot}01$ or better.

METHODS

Wavelet analysis

The wavelet analysis in this paper follows the methods of Torrence and Compo (1998). The software used was provided by C. Torrence and G. Compo, and is available at URL: http://paos.colorado.edu/research/wavelets/. Although the basic components and methods of wavelet analysis are reviewed here, readers are referred to Torrence and Compo (1998) for a more detailed explanation of the analysis.

The continuous wavelet transform and wavelet functions

The wavelet transform was designed to analyse time series that contain non-stationary power over many different frequency scales (Daubechies, 1990) and is most easily understood when compared with the more commonly used Fourier transform. The Fourier transform breaks up a signal into sine waves, and expresses a signal in terms of the frequency (x) and power (y) of its constituent sine waves, without reference to when the frequencies occur. Localization in time can be achieved with the Fourier transform by transforming the data within a specified window of time and shifting this window along the time series (Daubechies, 1992). However, the window length has to remain fixed regardless of the frequency. The *wavelet transform* addresses this problem by breaking up a signal into scaled versions of a *wavelet function*, where the scale of the wavelet (the window) varies with frequency. Thus, the wavelet is narrow in time at high frequencies and the scale of the wavelet increases with decreasing frequency. The wavelet transform, therefore, expresses a time series in three-dimensional space: time (x), scale/frequency (y), and power (z).

The wavelet transform may be continuous where the transform is calculated for all scales and positions in time, or discrete where the transform operates on discrete dyadic scales and positions in time. The continuous transform is used in this study. The *continuous wavelet transform* of a discrete time series x_n is defined as

$$W_n(s) = \sum_{n'=0}^{N-1} x_{n'} \psi^* \left[\frac{(n' - n)\delta t}{s} \right] \tag{1}$$

where N is the number of points in the time series, $\psi(t)$ is the wavelet function (normalized to have unit energy) at scale s and translated in time by n, δt is the time step for the analysis, and the asterisk indicates the complex conjugate (Torrence and Compo, 1998). Equation (1) is therefore the convolution of x_n with a scaled and translated version of the wavelet function. However, the calculation of the wavelet transform is much more efficient if the convolution is done in Fourier space using the Fourier transform (Torrence and Compo, 1998):

$$W_n(s) = \sum_{k=0}^{N-1} \hat{x}_k \hat{\psi}^* (s\omega_k) e^{i\omega_k n \delta t} \tag{2}$$

where $\hat{x}_k$ is the Fourier transform of x_n, k is the frequency index $(0, \ldots, N-1)$, and $\psi(s\omega_k)$ is the Fourier transform of the wavelet function at scale s and angular frequency ω_k.

A *wavelet function* is a waveform that has a zero mean and can be localized in both time and frequency space (Misiti *et al*., 1996). Numerous wavelet functions exist, and the choice of a function depends on both the desired analysis and the nature of the time series being analysed. Wavelet functions can be either orthogonal or non-orthogonal, and they can be complex- or real-valued functions. Orthogonal wavelets can only be used for discrete wavelet analysis, whereas non-orthogonal wavelets can be used for either discrete or continuous wavelet analysis. If the analysis requires information about the phase relationship between the wavelet spectra of two series, a complex wavelet (with real and imaginary parts) must be used. Two other aspects that should be considered when choosing a wavelet function are the width and the shape of the function. The shape of the function should reflect the features present in the data series (Smith *et al*., 1998; Torrence and Compo, 1998), and the width of the wavelet will depend on whether one is looking for good resolution in time or in frequency (Torrence and Compo, 1998). The work presented in this paper uses the Morlet wavelet:

$$\psi(t) = \pi^{-1/4} e^{i6t} e^{-t^2/2} \tag{3}$$

The Morlet wavelet, as shown in Equation (3), is the equation used by Torrence and Compo (1998). It is non-orthogonal and complex.

Local wavelet spectrum (variance) and cross-wavelet spectrum (covariance)

The *local wavelet power spectrum* (Torrence and Compo, 1998) is defined as the squared absolute value (or squared amplitude) of the wavelet transform coefficients ($|W_n(s)|^2$). The square of the absolute value ($|z|^2$) of a complex number ($z = a + b\mathrm{i}$) is simply the product of the number and its complex conjugate ($zz^* = (a + b\mathrm{i})(a - b\mathrm{i}) = a^2 + b^2$). Therefore, the *local wavelet power spectrum* is expressed as

$$W_n^{XX}(s) = W^X(s) W^{X*}(s) = |W_n^X(s)|^2 \tag{4}$$

where, again, the asterisk denotes the complex conjugate. When the wavelet function is complex (e.g. the Morlet), the wavelet transform coefficients are also complex. The values of the wavelet spectrum represent the magnitude of the variance in the series at a given wavelet scale and location in time.

When comparing two series x_n and y_n, the *local cross-wavelet spectrum* (or covariance) of the two series can be determined:

$$W_n^{XY}(s) = W_n^X(s) W_n^{Y*}(s) \tag{5}$$

Another useful property of the cross-spectrum of two series is the *phase difference* between the two series:

$$\theta_n^{XY}(s) = \tan^{-1}(\Im\{W_n^{XY}(s)\}/\Re\{W_n^{XY}(s)\}) \tag{6}$$

where $\Im\{W_n^{XY}(s)\}$ and $\Re\{W_n^{XY}(s)\}$ are the imaginary and real parts of the cross-wavelet spectrum respectively (Torrence and Compo, 1998). The phase is given in degrees (0–180°), where a 180° phase difference means the two series are completely out of phase. Therefore, at a scale of 24 h, the dependent variable lags the independent variable by 12 h.

Since the wavelet spectrum presents a large amount of information in one image, it is often desirable to condense this information by averaging the results over a range of scales or times. One useful technique is to average the variance at every scale over the whole time series, to compare the spectral power at different scales. Torrence and Compo (1998) call this the 'global wavelet spectrum'. The result is a graph of variance versus scale, analogous to the Fourier power spectrum, in which localization in time is lost. The *global wavelet spectrum* is defined as

$$\overline{W}_n^{XX}(s) = \frac{1}{N}\sum_{n=0}^{N-1} W_n^{XX}(s) \tag{7}$$

where N is the length of the series x. It is also often desirable to extract the results for a single wavelet scale, especially if the wavelet power is located in a limited number of scales.

Significance levels

The significance of the wavelet power spectrum can be evaluated by comparing the spectra with a background (or noise) spectrum. The background spectrum depends on the nature of the data. In geophysical processes the background spectrum is often either white noise (constant variance across all scales, or frequencies) or red noise (increasing variance with increasing scale, or decreasing frequency) (Schiff, 1992; Torrence and Compo, 1998). Once the background spectrum is chosen, the wavelet spectrum of the time series is compared with the expected spectrum of the background function at a determined confidence level. Where the wavelet power of the time series exceeds the power of the background at the chosen confidence level, the time series variance can be deemed significant relative to the expected background. The calculation of the background spectrum depends on the type of wavelet spectrum being evaluated: local, global, or cross spectrum (Torrence and Compo, 1998). For example, the distribution of the normalized local wavelet power spectrum is

$$\frac{W_n^{XX}(s)}{\sigma_x^2} \Rightarrow \frac{1}{2}P_k\chi_2^2 \tag{8}$$

at each time t and scale a. The value of P_k is the mean Fourier power of the background spectrum for the Fourier frequencies k that correspond to the wavelet scales s, and χ_2^2 is the chi-square value for the chosen confidence level (e.g. 95%), where the subscript '2' on χ^2 designates the degrees of freedom (two for a complex wavelet and one for real-valued functions). The Fourier power P_k of a white noise spectrum is equal to one at all k. For the red noise spectrum, the Fourier spectrum is (Torrence and Compo, 1998)

$$P_k = \frac{1-\alpha^2}{1+\alpha^2-2\alpha\cos(2\pi k/N)} \tag{9}$$

where α is the assumed lag-1 autocorrelation for the time series.

The next section explains how the wavelet analysis tools described above were applied to the data collected at Bow Lake between 1997 and 2000.

Wavelet analysis of discharge and temperature time-series

The Morlet wavelet was chosen for this analysis, because it is complex and thus allows for the determination of the phase relationship between the temperature and discharge series. The Morlet wavelet also has relatively

good resolution in frequency compared with other wavelets, such as the Mexican Hat or Paul, which have better resolution in time. Furthermore, the wavelet is smooth and symmetrical, similar to the features in the temperature and discharge time series. It has also been used previously in both hydrological and meteorological applications (Torrence and Compo, 1998; Labat *et al.*, 2000).

The start date and total length of the stream discharge and temperature measurements varied from year to year. To simplify inter-annual and inter-stream comparisons of the wavelet analyses, the time series were truncated to keep the start and end dates consistent. The series were confined to the latest start date (7 June, day 157), and the earliest end date (3 September, day 247) for a total series length of 2130 h, or 88·75 days. The only exception to this is the 1997 hourly temperature record, which ends on 30 August 1997. Since the temperature and discharge time series have widely different statistics, the series were also centred on their means and normalized by their standard deviations prior to calculating the wavelet transforms to facilitate comparison of results across catchments and years. The hourly precipitation data from 1999 and 2000 were not normalized because the large number of zeros in these time series meant that the data were not normally distributed.

The wavelet transform was calculated for a discrete set of 42 ($j = 0, 1, \ldots, 41$) scales. The scales are a series of fractional powers of two (Torrence and Compo, 1998):

$$s_j = s_0 2^{j\delta j} \tag{10}$$

where $s_0 = 6$ h and $\delta j = 0{\cdot}125$. This gives scales ranging from 6 h to 209 h (approximately 9 days). It should be noted that the wavelet scale is often expressed in terms of its equivalent Fourier period in order to facilitate the comparison of the wavelet and Fourier power spectra. The scale–period relationship varies for different wavelet functions, and the equivalent Fourier period for a particular wavelet can be derived analytically (Torrence and Compo, 1998). For the Morlet wavelet the wavelet scale and Fourier period are almost equal (Period = 1·03 × Scale), so the terms period and scale are used interchangeably here.

The red-noise spectrum was chosen as the background spectrum for testing the significance of the results, since the data match this spectrum quite well. A lag-1 autocorrelation coefficient (α in Equation (9)) of 0·96 was found for all four temperature series (1997–2000), but α values for the runoff time series varied between each year. Their values are presented in Table I. For the wavelet analysis of rainfall, a white noise spectrum was used as the background ($\alpha = 0$).

The local wavelet power spectra $W_n^{QQ}(s)$ or $W_n^{TT}(s)$, the global wavelet spectra $\overline{W}_n^{QQ}(s)$ or $\overline{W}_n^{TT}(s)$, and the corresponding 95% confidence levels for the red-noise spectra were determined for each of the discharge series (four for the glacial stream (Q_{GL}) and four for the Bow River (Q_{BR})) and temperature series (T) for the summers (June–August) 1997 to 2000. The local wavelet cross-spectra $W_n^{TQ}(s)$ and the phase coherence $\theta_n^{TQ}(s)$ (or lag) were then determined for the paired temperature (independent variable) and runoff (dependent variable) series for each year. The local precipitation–runoff wavelet cross-spectra $W_n^{PQ}(s)$ and the phase coherence $\theta_n^{PQ}(s)$ were also determined for 1999 and 2000.

RESULTS

A summary of seasonal snow, temperature, and rainfall conditions illustrates the inter-annual variability in the gross hydroclimatological conditions at Bow Lake in the period 1997–2000 (Table II). The year fall 1997

Table I. The lag-1 autocorrelation coefficients α used for testing significance of the wavelet power

	1997	1998	1999	2000
α_{GL}	0·93	0·98	0·99	0·999
α_{BR}	0·97	0·99	0·99	0·997

Table II. Comparison of seasonal snowpack, temperature, and precipitation conditions at Bow Lake for 1997–2000

	1996–97	1997–98	1998–99	1999–2000
Snowpack (mm SWE) at Bow Summit (2080 m a.s.l.)				
30 March	462	257	460	434
30 May	254	0	329	239
Exhaustion of snowpack at Bow Lake met. station (1940 m a.s.l.)	—	2 May	30 May	23 May
Discharge (10^6 m^3)				
Bow River (7 June–31 August)	7·7	4·1	8·1	7·5
June	3·5	1·9	2·9	2·5
July	2·7	1·8	3·5	3·6
August	1·5	0·9	1·8	1·4
Glacial (7 June–31 August)	28	34	20	19
June	9·0	5·3	3·5	2·7
July	9·3	15	6·7	8·9
August	9·4	13	9·5	7·1
Degree-day total (°C) January–August	838	1148	791	808
Mean daily air temp. (°C)				
May	2·4	5·5	0·9	1·3
June	6·1	6·8	5·3	6·0
July	9·1	12·6	7·8	9·6
August	9·2	11·1	10·5	8·6
Total precipitation (mm) June–August	193	233	236	155
Total monthly precipitation (mm)				
June	59·8	82·0	27·5	41·7
July	63·4	40·4	117·1	82·8
August	69·8	110·4	91·5	30·8

to fall 1998 had much lower snowfall, and higher spring and summer temperatures than all the other years. According to monthly snow course measurements at Bow Summit by Alberta Environment (Figure 1), the snow accumulation (mm SWE) at the end of March 1998 was approximately 57% of that in March 1997, 1999, and 2000. The positive degree-day total (1 January–3 September), a measure of energy input during the melt season, was 26–30% higher in 1998 than in the other years. 1999 was the coldest summer, and winter 1998–99 had the highest snowpack SWE. In 1998, the glacial stream had the highest total seasonal runoff of the four years ($3{\cdot}4 \times 10^7$ m^3), and the Bow River had the lowest total runoff that year ($4{\cdot}1 \times 10^6$ m^3). In the case of the Bow River, seasonal runoff increased with increasing snowpack SWE (Table II). For the glacial stream, seasonal discharge increased with increasing temperature (positive degree-day total) and decreasing snowpack (SWE; Table II).

Figure 2 and Table III present the results of the global wavelet analysis of the discharge and air temperature time series for 1997–2000. The power of the global wavelet spectra is the variance averaged at each scale across the whole length of the time series. Since the data series were mean centred and normalized, the spectral power is dimensionless. Therefore, the wavelet *power* expresses the *variance of the series* as squared standard deviations from the mean. The terms variance and power are used interchangeably in the text. The 95% confidence level for a red-noise spectrum (the significance line) was determined for each spectrum. In order to avoid cluttering the graphs, only the significance lines for the 1997 ($\alpha_{GL} = 0{\cdot}93$ and $\alpha_{BR} = 0{\cdot}97$) and 2000 ($\alpha_{GL} = 0{\cdot}999$ and $\alpha_{BR} = 0{\cdot}997$) series were plotted. The α values are highest for 2000 because the signal is very smooth, and the autocorrelation of the data is very strong at a 1 h lag. The lower α values for 1997 indicate that the discharge signal is noisier than for other years (Table I). As a result, the significance

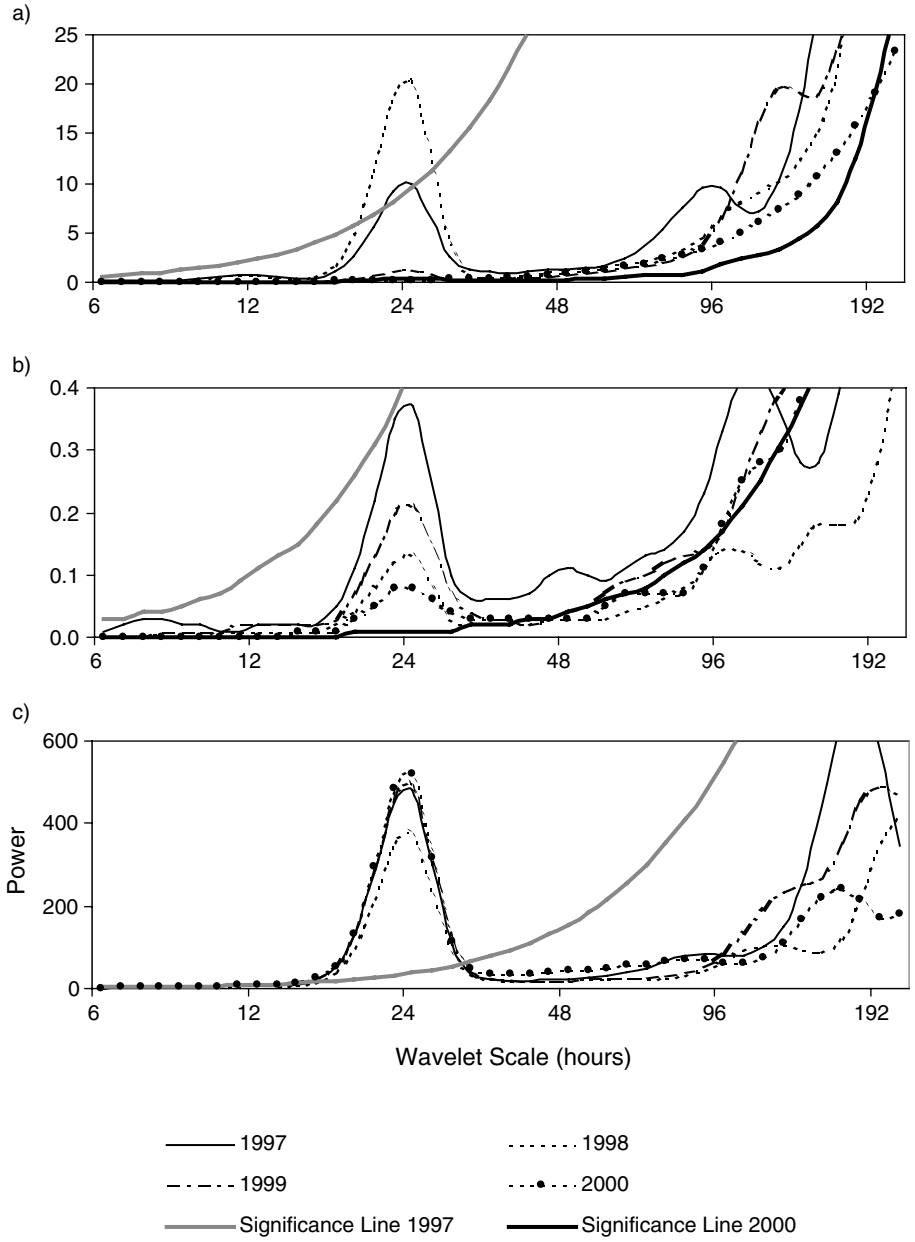

Figure 2. Plot of global spectra for each year by variable: (a) glacial stream discharge; (b) Bow River discharge; (c) air temperature

lines for the background spectrum in 1997 are higher than in other years, and the variance in the discharge series has to be much stronger in order to be considered significant.

The power around the 24 h scale is the dominant feature in all the global spectra, indicating strong diurnal signatures in the time series. There is also high power at low frequency (96 < 192 h) in all years, indicating strong signals at the scale of weather systems (4–8 days), but the power is not usually significant at these scales (Figure 2, Table III). For the glacial stream, the diurnal signal was strongest in 1998 and then 1997 (Figure 2a, Table III). In 1999 and 2000, the power of the diurnal signal was orders of magnitude lower

Table III. Summary of results from the global wavelet spectra for runoff Q and temperature T for the 24 h scale $\overline{W}_n^{XX}(24)$ and for the mean low-frequency power centred on 120 th ($\overline{W}_n^{XX}(120)$ the average global power for scales between 96 and 148 h). The ratio of the global power for discharge at the 24 h scale in the two streams is also shown ($\overline{W}_n^{QQ}(24)$ GL/BR). The last column lists the day when the normalized Bow River discharge falls below zero (Q_{BR} norm < 0) for each year

	Glacial		Bow River		Temperature		GL/BR	Q_{BR} norm < 0
	$\overline{W}_n^{QQ}(24)$	$\overline{W}_n^{QQ}(120)$	$\overline{W}_n^{QQ}(24)$	$\overline{W}_n^{QQ}(120)$	$\overline{W}_n^{TT}(24)$	$\overline{W}_n^{TT}(120)$	$\overline{W}_n^{QQ}(24)$	
1997	9·9	13	0·37	0·35	480	183	27	205
1998	20	10	0·13	0·14	370	91	154	194
1999	1·3	15	0·22	0·35	500	194	6	211
2000	0·42	3	0·08	0·33	520	117	5	216

than in 1998. The wavelet power at the 12 h scale was also significant for the glacial stream runoff in 1998 (Figure 2a). For the glacial stream, the mean low-frequency global power centred on 120 h ($\overline{W}_n^{QQ}(120)$), was greater than the 24 h scale power $\overline{W}_n^{QQ}(24)$ in all years except 1998 (Table III). The magnitude of the diurnal and low-frequency power was always higher for the glacial stream than for the Bow River (Table III). This implies that the glacial stream discharge is more responsive to temperature changes, both at diurnal time scales and at the scale of weather systems.

The distribution of global power across scales is similar for the two streams, but the magnitude of the power is much lower for the Bow River (Figure 2b). The global diurnal power for the Bow River runoff was most pronounced in 1997, followed by 1999 (Table III). However, despite the magnitude of the power, the global variance in the Bow River runoff at the 24 h scale was not statistically significant in 1997, due to the noise in the record (Figure 2b). The 12 h scale variance in runoff was significant for this stream in 1998, 1999, and 2000. The average low-frequency power for the Bow River was generally of the same order of magnitude as the diurnal scale power, and was lowest in 1998 (Table III). The global wavelet spectra for temperature are similar to the stream discharge spectra, but the power is orders of magnitude higher (Figure 2c, Table III). The power is very strong at the 24 h scale, and there is little variability from year to year. The power is also strong at low frequencies, where it displays greater inter-annual variability (Figure 2c, Table III).

The temperature and discharge time series are shown in Figures 3–6, along with their local wavelet spectra. The significant features of the wavelet analyses are also summarized by stream and year in Table IV. As for the global spectra, most of the variance in the local spectra is concentrated at the 24 h scale, although periodically there is significant variance at sub-diurnal scales (Figures 3a–c(ii)–6a–c(ii)) and also at higher scales (Figures 3c(ii), 5a(ii), and 6a(ii)). For the glacial stream, the low-frequency power (>96 h) is usually strongest in July and August (Figures 3a(ii)–6a(ii)). For the Bow River discharge, the power at low frequency is strongest in June and early July, but is never statistically significant, and always much lower than for the glacial stream discharge (Figures 3b(ii)–6b(ii)). The diurnal component of the local wavelet spectra for air temperature is much more consistent in strength and distribution in time than the low-frequency power (e.g. Figure 3c(ii)). The diurnal power for the discharge spectra is much weaker than for air temperature, and there is greater seasonal and inter-annual variability in the distribution of the 24 h discharge signal (Figures 3–6).

In 1997, the local wavelet spectra for runoff in both streams had significant power at the 24 h and 6–12 h scales near the beginning of June (Figure 3a(ii) and b(ii), days 158–170). This power increased moderately in both streams between the end of July and end of August, but it was not significant (Figure 3a(ii) and b(ii), days 195–240). In 1998, the 24 h wavelet power for discharge in both streams was concentrated between mid July and August, with frequent episodes of significant power at the 6 and 12 h scales, especially in August (Figure 4a(ii) and b(ii), days 190–248). The power in the diurnal discharge cycle was always higher in the glacial stream than in the Bow River in 1997 and 1998 (Figures 3, 4, 7d, and 8d). In 1999 and 2000, the diurnal signal in glacial stream discharge was much weaker than in 1997 and 1998, but the variance was still

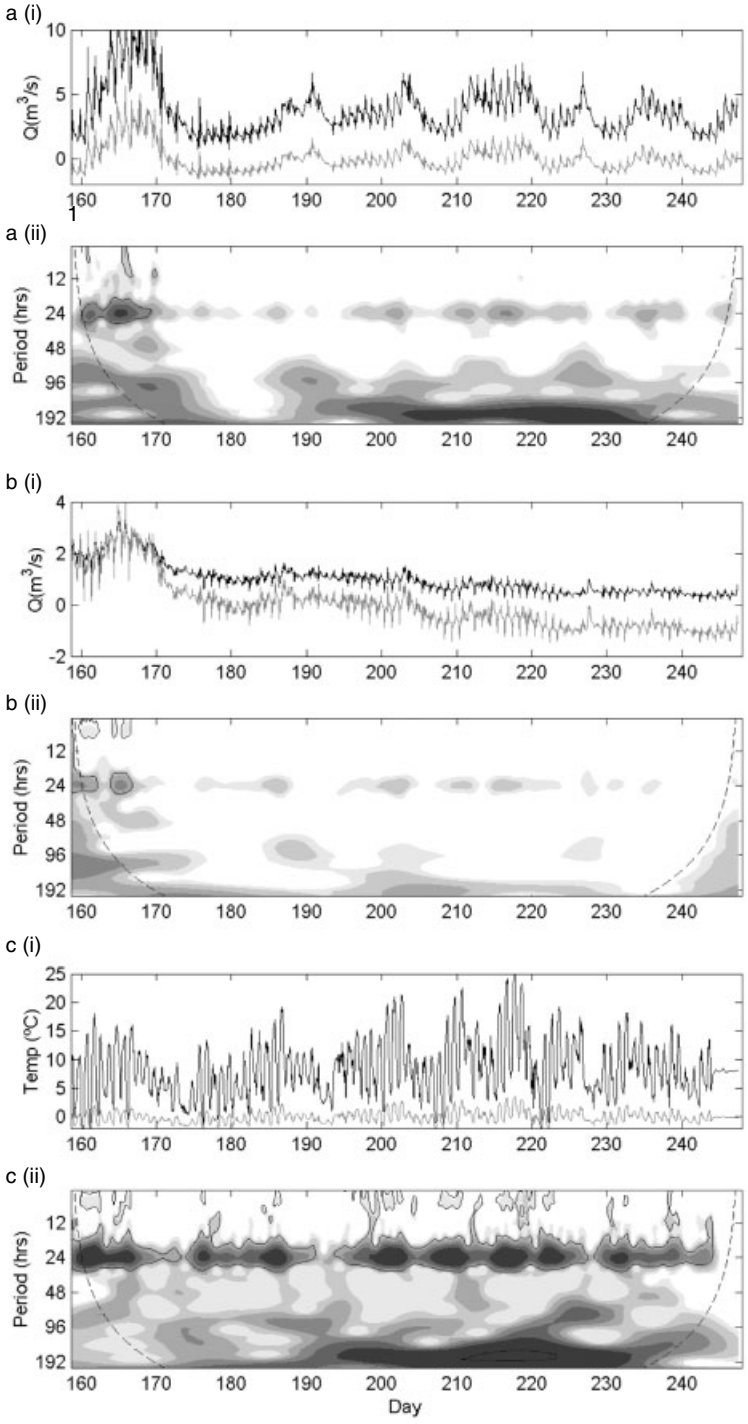

Figure 3. Time series and wavelet spectra for 1997: (a) glacial stream discharge; (b) Bow River discharge; (c) air temperature. (i) The raw time series (black) and the mean centred and normalized time series (grey). (ii) Wavelet power spectrum $W_n^{XX}(s)$ contoured at variance 0·5, 1, 2·5, 5, 10, and 20 (light to dark grey). The black line contours the areas where the power is considered significant (i.e. exceeds the 95% confidence level of a red-noise process), the dashed black line delineates the cone of influence (COI)

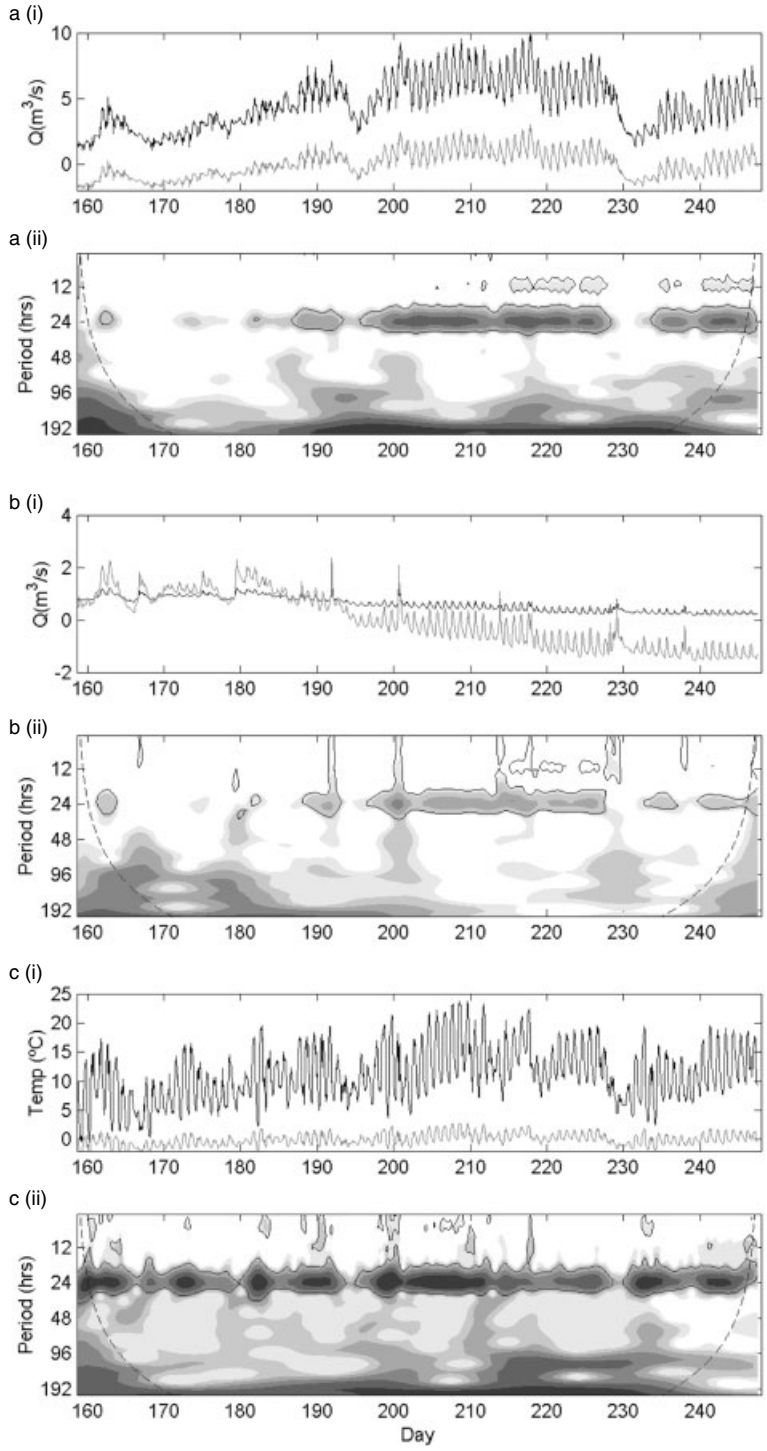

Figure 4. Time series and wavelet spectra for 1998: (a) glacial stream discharge; (b) Bow River discharge; (c) air temperature. (i) The raw time series (black) and the mean centred and normalized time series (grey). (ii) $W_n^{XX}(s)$ contoured at variance 0·5, 1, 2·5, 5, 10, and 20 (light to dark grey). The black line contours the areas where the power is considered significant; the dashed black line delineates the COI

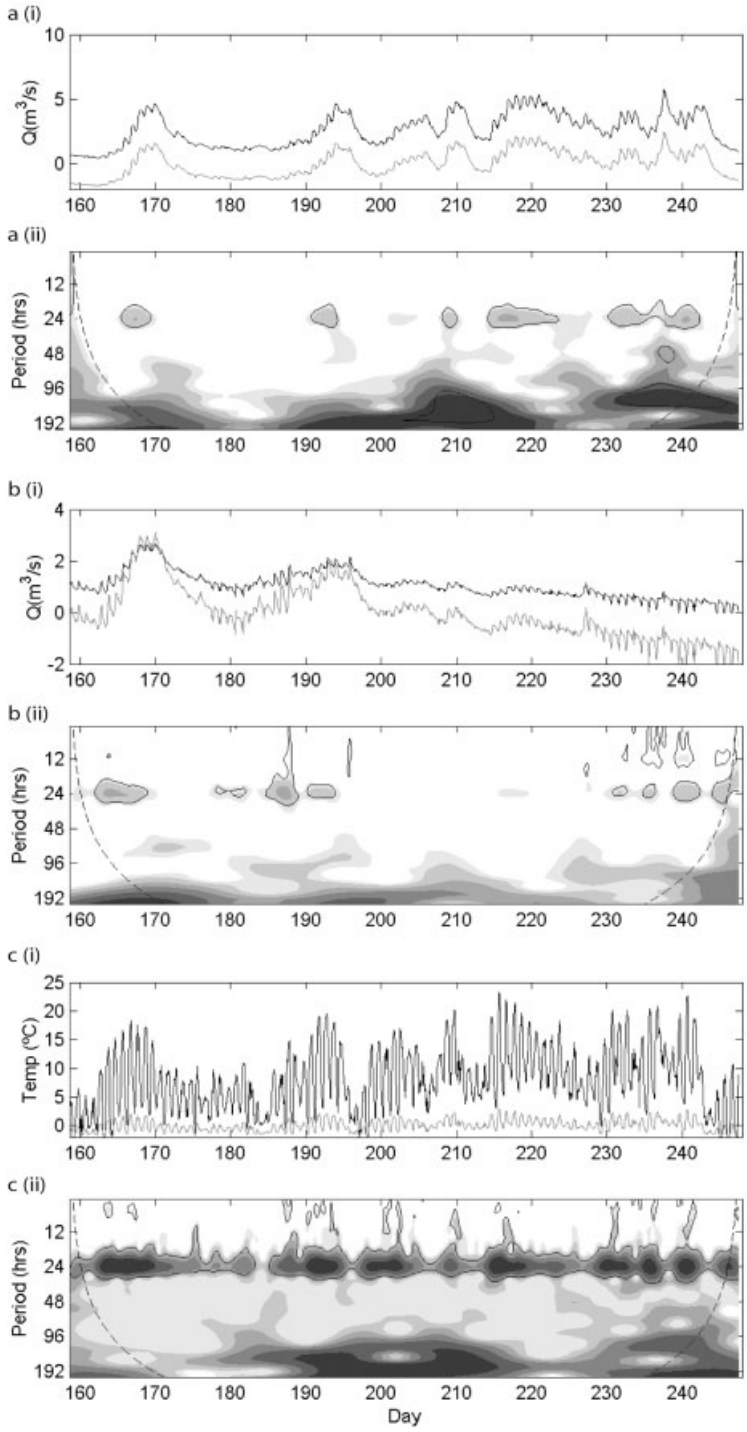

Figure 5. Time series and wavelet spectra for 1999: (a) glacial stream discharge; (b) Bow River discharge; (c) air temperature. (i) The raw time series (black) and the mean centred and normalized time series (grey). (ii) $W_n^{XX}(s)$ contoured at variance 0·5, 1, 2·5, 5, 10, and 20 (light to dark grey). The black line contours the areas where the power is considered significant; the dashed black line delineates the COI

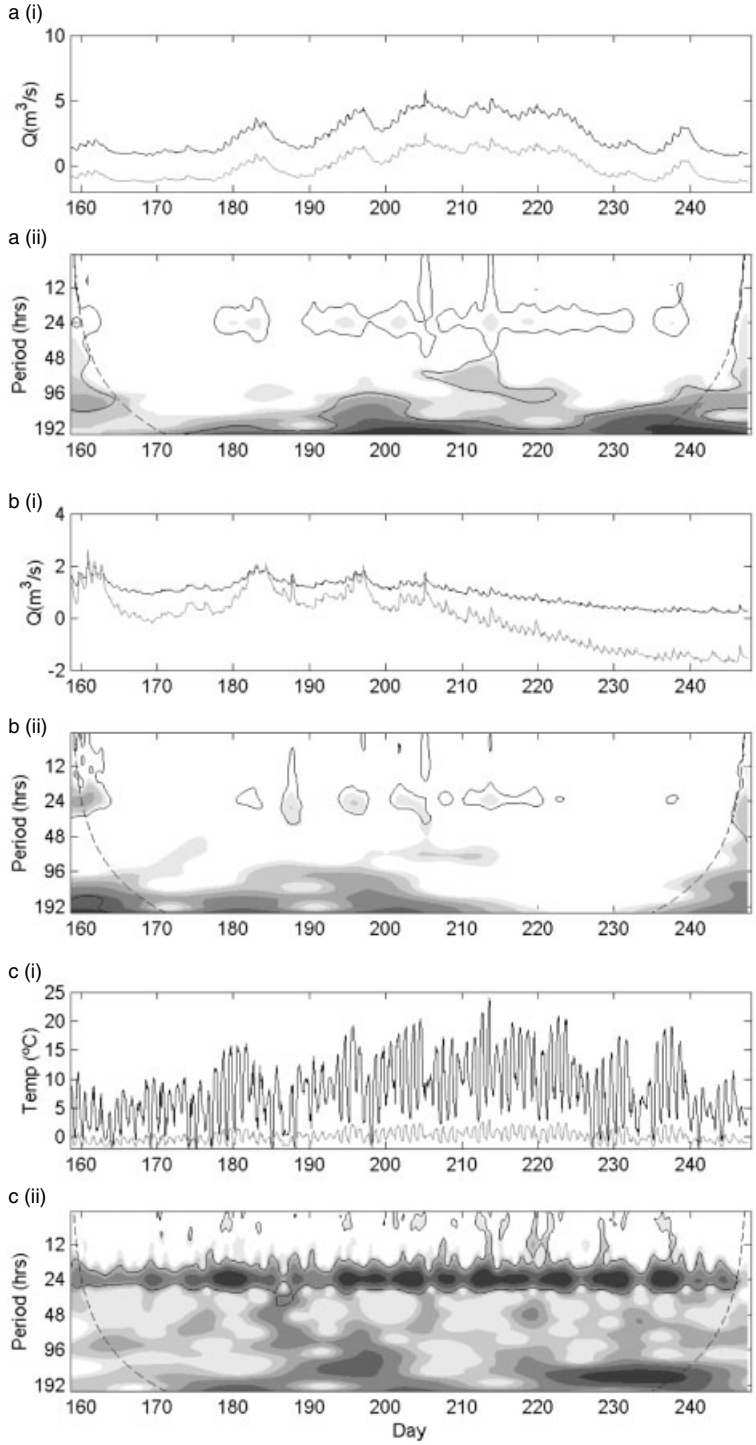

Figure 6. Time series and wavelet spectra for 2000: (a) glacial stream discharge; (b) Bow River discharge; (c) air temperature. (i) The raw time series (black) and the mean centred and normalized time series (grey). (ii) $W_n^{XX}(s)$ contoured at variance 0·5, 1, 2·5, 5, 10, and 20 (light to dark grey). The black line contours the areas where the power is considered significant; the dashed black line delineates the COI

Table IV. Summary of key features of wavelet analysis by stream and year. The time of occurrence of the key features are indicated by day

Feature	1997		1998		1999		2000	
	GL	BR	GL	BR	GL	BR	GL	BR
Strong $W_n^{QQ}(24)$	160–170	160–170	162–164/ 186–248	161–165/ 187–248	167–170/ 191–193/ 210–220/ 230–243	163–170/ 179–193/ 230–247	178–184/ 189–233	160–165/ 180–189/ 195–220
Strong $W_n^{QQ}(<24)$	162/167	160–167	215–228/ 235–248	168/179/ 192/201/ 215–230/ 238		163/188/ 196/ 232–245	205/213	160–164/ 188/198/ 205/213
Significant $W_n^{QQ}(>96)$					203–215/ 231–247		174–245	
Strong $W_n^{QQ}(s)$, no strong $W_n^{TQ}(s)$	168		215–228/ 235–237	168/179/ 215–230/ 238	237–239	163/196/ 228–245	205–222	160–164/ 188/198/ 205
Mean $\theta^{TQ}(24)$ (h)	5·4	4·9	5	3·6	6·3	7·4	7·1	5·6
Rapid change in $\theta^{TQ}(24)$	192–195	192–195	241–244	168–170/ 178–181/ 228–229	237–239	223–225	186–188/ 204–206	174–177/ 184–186/ 197/ 204–206

statistically significant, especially during July and August (Figure 5a(ii), days 210–240; Figure 6a(ii), days 190–220). In 1999, the 24 hour power in the Bow River was highest in June and again at the end of August (Figure 5b(ii)), and in 2000 it was strongest in early June and then increased occasionally, particularly during July (Figure 6b(ii)).

The local temperature–runoff cross-wavelet spectra mimic the general patterns present in the local wavelet spectra for discharge (Figures 7–10). Since the temperature consistently displays strong variance at the diurnal scale in the local spectra, the seasonal and inter-annual variability in the local temperature–runoff cross-wavelet spectra is a lot lower than in the local spectra of the discharge series. The local cross-wavelet spectrum can have significant coherence in places where only one of the paired local wavelet spectra displays a significant signal (e.g. cf. Figures 7 and 3). Hence the local cross-wavelet spectra and the corresponding local wavelet spectra should be examined together, to determine whether the 'significant' covariance is actually meaningful in terms of the runoff variance. The significance contours for local wavelet power in the discharge series, therefore, are plotted on each of the local cross-wavelet spectra to show when the strong temperature–discharge covariance coincides with significant variance in stream runoff. The phase difference at the 24 h scales is shown in Figures 7c–10c.

In general, the temperature–discharge covariance for both streams is concentrated at the 24 h time scale, and sometimes at shorter time scales (Figures 7–10). There is also strong covariance at higher scales for the glacial stream (Figures 7a, 9a, and 10a). When discharge showed strong variability at the 24 h and higher scales, it was usually strongly covariant with temperature (Figures 7a and b–10a and b). However, at shorter (6–12 h) time scales, discharge often showed strong variability in the absence of strong covariance with temperature. This was especially true for the Bow River in 1999 (Figure 9b, days 196, 227–248) and 2000 (Figure 10b, days 158–164, 188, 198, 205), and for both streams in 1998 (Figure 8a and b, days 210–225). These episodes of high variance in discharge at the lower scales appear to be related to precipitation events.

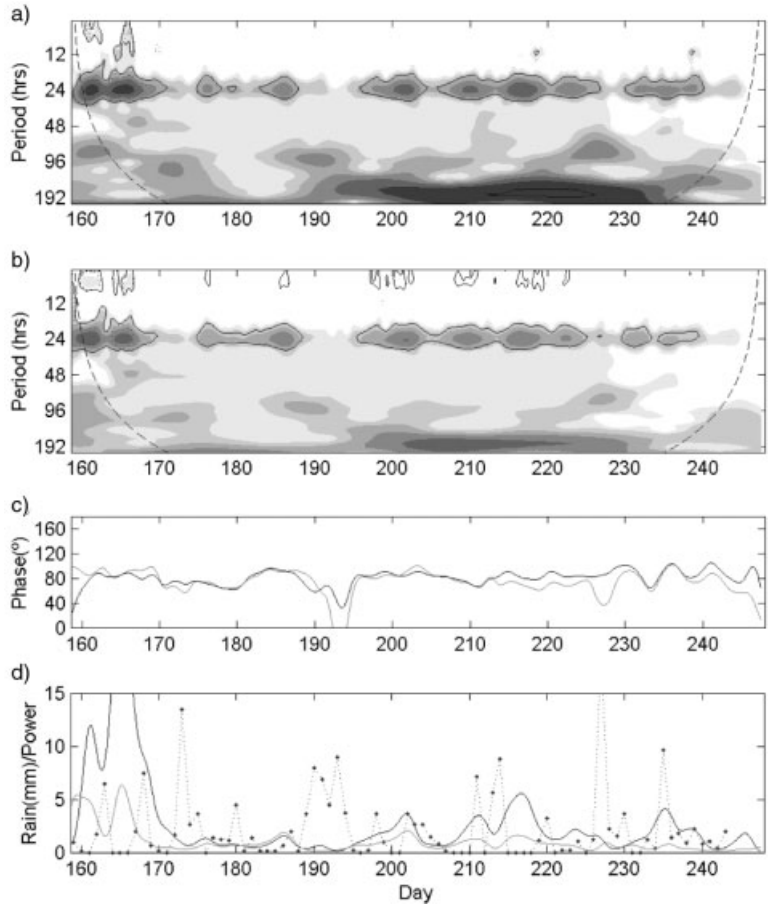

Figure 7. Cross-wavelet analysis 1997. (a) Temperature and glacial discharge cross-spectral analysis, $W_n^{TQ_{GL}}(s)$. (b) Temperature and Bow River cross-spectral analysis, $W_n^{TQ_{BR}}(s)$, with contours at variance 0·5, 1, 2·5, 5, 10, 20. The black contour line is the 95% confidence level of the cross-spectrum, the dashed contour is the 95% confidence level of the local discharge spectrum, and the dashed black line on the edges is the COI. (c) The phase difference (or lag) at the 24 h scale, $\theta_n^{TQ}(24)$, for GL (black), and BR (grey). (d) Wavelet power spectrum for discharge at the 24 h scale, $W_n^{QQ}(24)$, for GL (black) and BR (grey) and daily total rainfall (dotted line with dots)

The phase difference between temperature and discharge at the 24 h scale was typically between 4–6 h (60–90°), and the Bow River discharge usually responded more quickly to temperature than the glacial stream, except in 1999 (Table IV). The phase differences for the two streams were very similar in 1997, when they did not exceed 6 h, and only fell below 4 h on one occasion (Figure 7c). In 1998, the phase differences for the two streams were less similar (Figure 8c), and the average phase differences for both streams were shorter than in all other years (Table IV). The lags were higher for both streams, between 6 and 9 h, for most of 1999 (Figure 9c, days 160–230) and 2000 (Figure 10c, days 160–215). The difference in lags between the two streams in 1999 was small until the end of August, when the glacial stream had a faster response (Figure 9c, days 228–248). In 2000, the Bow River discharge usually had shorter lag times than the glacial stream, especially in June (Figure 10c, days 160–188). Another key feature of the phase difference graphs is the irregular, sudden, and dramatic changes (Figures 7c–10c). These large drops and/or increases in lag were generally short lived and appeared to coincide with precipitation events. They were more frequent and more pronounced for the Bow River than for the glacial stream.

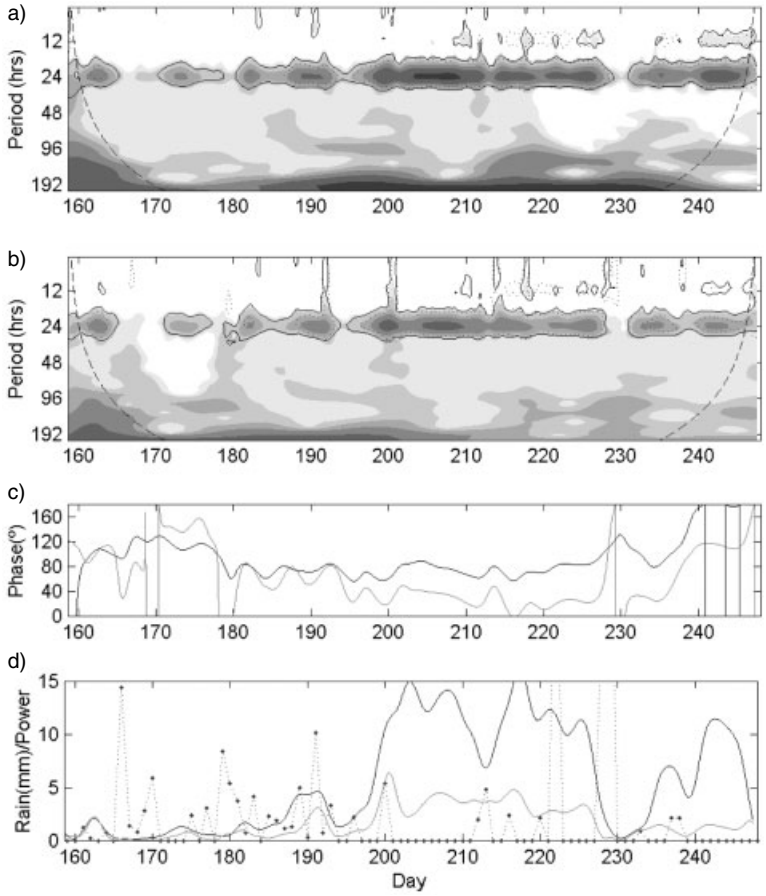

Figure 8. Cross-wavelet analysis 1998. (a) $W_n^{TQ_{GL}}(s)$. (b) $W_n^{TQ_{BR}}(s)$ with contours at variance 0·5, 1, 2·5, 5, 10, 20. The black contour line is the 95% confidence level of the cross-spectrum, the dashed contour is the 95% confidence level of the local discharge spectrum, and the dashed black line on the edges is the COI. (c) $\theta_n^{TQ}(24)$ for GL (black), and BR (grey). (d) $W_n^{QQ}(24)$ for GL (black) and BR (grey) and daily total rainfall (dotted line with dots)

The abrupt disruptions in the phase diagrams led to the investigation of precipitation–discharge relationships. Since the hourly precipitation records for 1997 and 1998 were discontinuous, the wavelet analysis of precipitation data was performed only for 1999 and 2000. The local wavelet spectra for precipitation and the local discharge–precipitation cross-wavelet spectra are illustrated in Figures 11 and 12. As for the discharge–temperature cross-spectra, the significance contours for local wavelet power of the discharge series are plotted on the discharge–precipitation cross-wavelet spectrum to illustrate when variance in discharge was significant. In addition, the local wavelet power for discharge and precipitation at the 24 h scale is plotted below the local cross-wavelet spectra (Figures 11e and 12e).

Unlike the local discharge and temperature spectra, where the power is concentrated at the 24 h scale, the power in the local rainfall spectra is spread out across the 6–192 h scales, depending on the duration of the event. There were more major precipitation events in 1999 than in 2000 (Figures 11b and 12b). Compared with the Bow River, the glacial stream shows little or weak covariance with precipitation (Figures 11 and 12). The response of the Bow River discharge to precipitation events appeared to be delayed by 1 or 2 days in June and early July (Figure 11d, days 183–188; Figure 12d, days 160–165, 185–188), but not later in the summer.

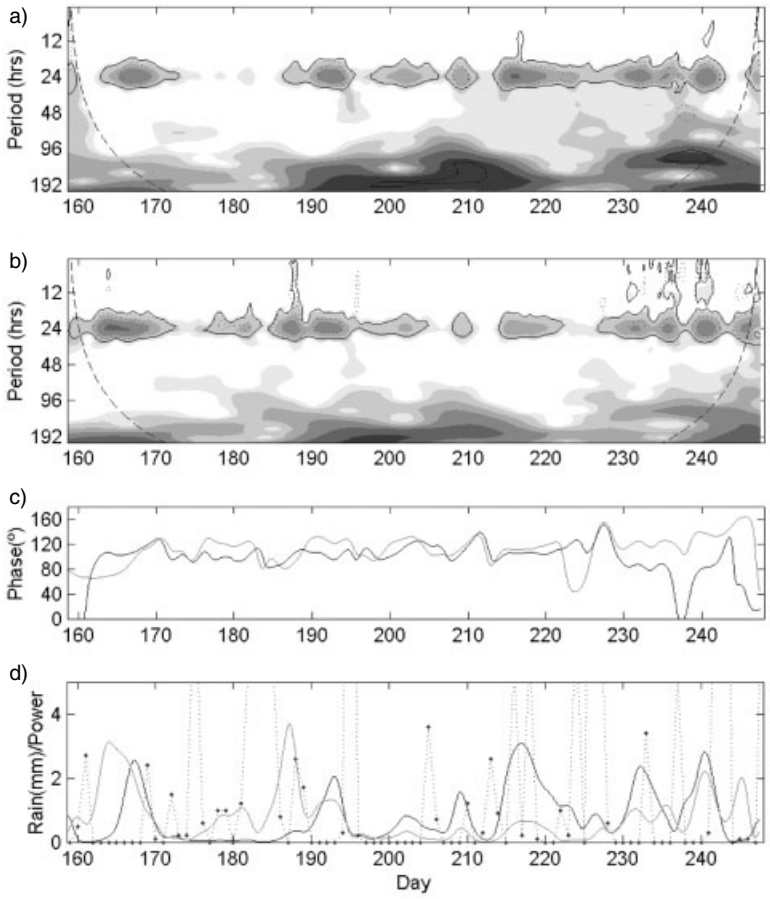

Figure 9. Cross-wavelet analysis 1999. (a) $W_n^{TQ_{GL}}(s)$. (b) $W_n^{TQ_{BR}}(s)$ with contours at variance 0·5, 1, 2·5, 5, 10, 20. The black contour line is the 95% confidence level of the cross-spectrum, the dashed contour is the 95% confidence level of the local discharge spectrum, and the dashed black line on the edges is the COI. (c) $\theta_n^{TQ}(24)$ for GL (black), and BR (grey). (d) $W_n^{QQ}(24)$ for GL (black) and BR (grey) and daily total rainfall (dotted line with dots)

DISCUSSION

Conceptual model for the hydrological interpretation of wavelet analyses

In glacial and nival catchments, spatial and temporal changes in water sources, and in hydrological storage and transfer processes, occur as a result of seasonal snow and ice melt. These seasonal changes in the hydrological system manifest themselves as changes in characteristics of the discharge hydrograph, and also as changes in the relationship between air temperature and discharge. The following discussion outlines the typical seasonal changes in the hydrological processes in the two types of catchment, and the features in the time series and wavelet analyses that can be used to identify shifts in hydrological behaviour.

Within a catchment there are seasonal changes in the relative contributions of different water sources to runoff. In an ice-free catchment, the dominant component of runoff shifts from snowmelt to rainfall and base flow. In a glacial catchment, snowmelt continues at higher elevations and is replaced by ice melt in the ablation zone, and by rainfall in ice-free areas. Changes in storage and flow routing also occur as snowmelt progresses. Early in the season, meltwater percolates into the snowpack and is stored or refrozen. Once the snowpack ripens, meltwater runoff begins. As the snowpack thins, the time required for meltwater to percolate from the

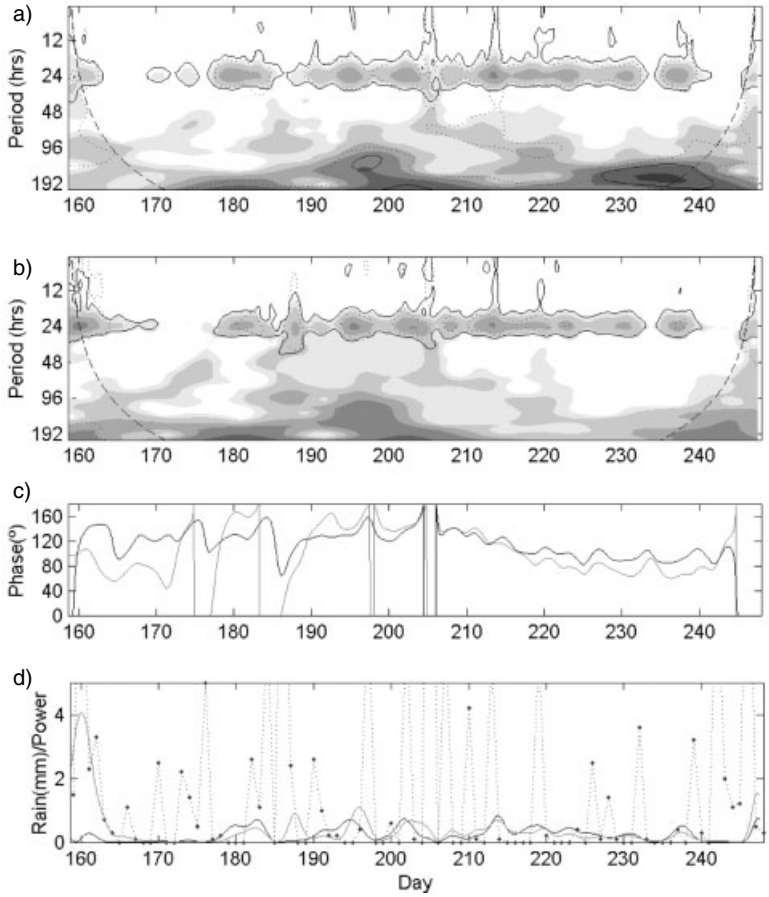

Figure 10. Cross-wavelet analysis 2000. (a) $W_n^{TQ_{GL}}(s)$ (b) $W_n^{TQ_{BR}}(s)$ with contours at variance 0·5, 1, 2·5, 5, 10, 20. The black contour line is the 95% confidence level of the cross-spectrum, the dashed contour is the 95% confidence level of the local discharge spectrum, and the dashed black line on the edges is the COI. (c) $\theta_n^{TQ}(24)$ for GL (black), and BR (grey). (d) $W_n^{QQ}(24)$ for GL (black) and BR (grey) and daily total rainfall (dotted line with dots)

melting surface to the base of the snowpack decreases (Fountain, 1996). At the start of the season, overland flow may be common over soils that are frozen at shallow depth. If soils thaw from the top down, then storage capacity gradually increases but deep flow paths are sealed off by pore ice at depth. Shallow subsurface and overland flow result as soils thaw and receive inputs from snowmelt and precipitation. This may continue until the ice at depth melts, and deep flow paths open. In a glacial catchment, the exposure of low-albedo ice and the resulting increase in the melt rate leads to the seasonal development of more efficient supraglacial, englacial, and subglacial drainage pathways (Richards *et al*., 1996). As a result, the glacial system becomes more responsive to meltwater inputs, especially later in the summer if major subglacial channels develop. The rapid response of the glacial system in 1998 is indicated by the strong power at the 12 h time scale (Figure 4). However, in the case of runoff from Bow Glacier, the proglacial lake is a potentially large storage reservoir (volume 9×10^6 m^3) that may dampen the variability of runoff from the glacier (Figure 1).

The seasonal changes in the dominant water sources, and storage and flow routing processes discussed above, can be identified using various features of the raw time series and wavelet analyses. The retreat of the seasonal snowpack in an ice-free catchment should result in a decrease in the amplitude of the diurnal discharge signal, a decrease in the responsiveness of discharge to longer scale (4–8 days) temperature variability, and

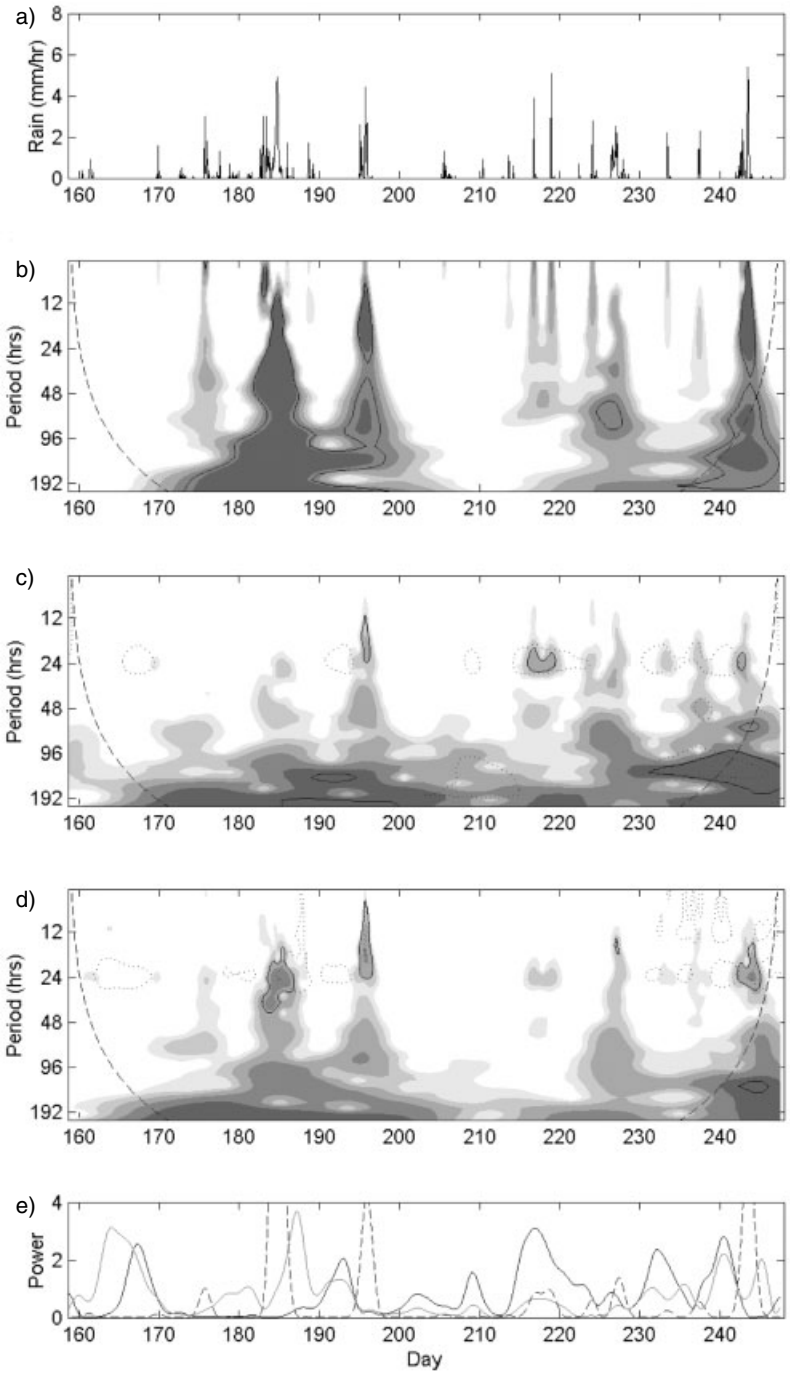

Figure 11. Wavelet analysis of hourly precipitation 1999: (a) hourly rain (mm); (b) $W_n^{PP}(s)$ contoured at variance 0·25, 0·5, 1, 2, and 4 (light to dark grey); (c) $W_n^{PQ_{GL}}(s)$; (d) $W_n^{PQ_{BR}}(s)$. The cross-wavelet spectrums are contoured at powers of 0·25, 0·5, 1·0, and 4·0. The black contour line is the 95% confidence level of the cross-spectrum, the dashed contour is the 95% confidence level of the local discharge spectrum, and the dashed black line on the edges is the COI. (e) $W_n^{PP}(24)$ (dashed), $W_n^{QQ}(24)$ for GL (black), and $W_n^{QQ}(24)$ BR (grey)

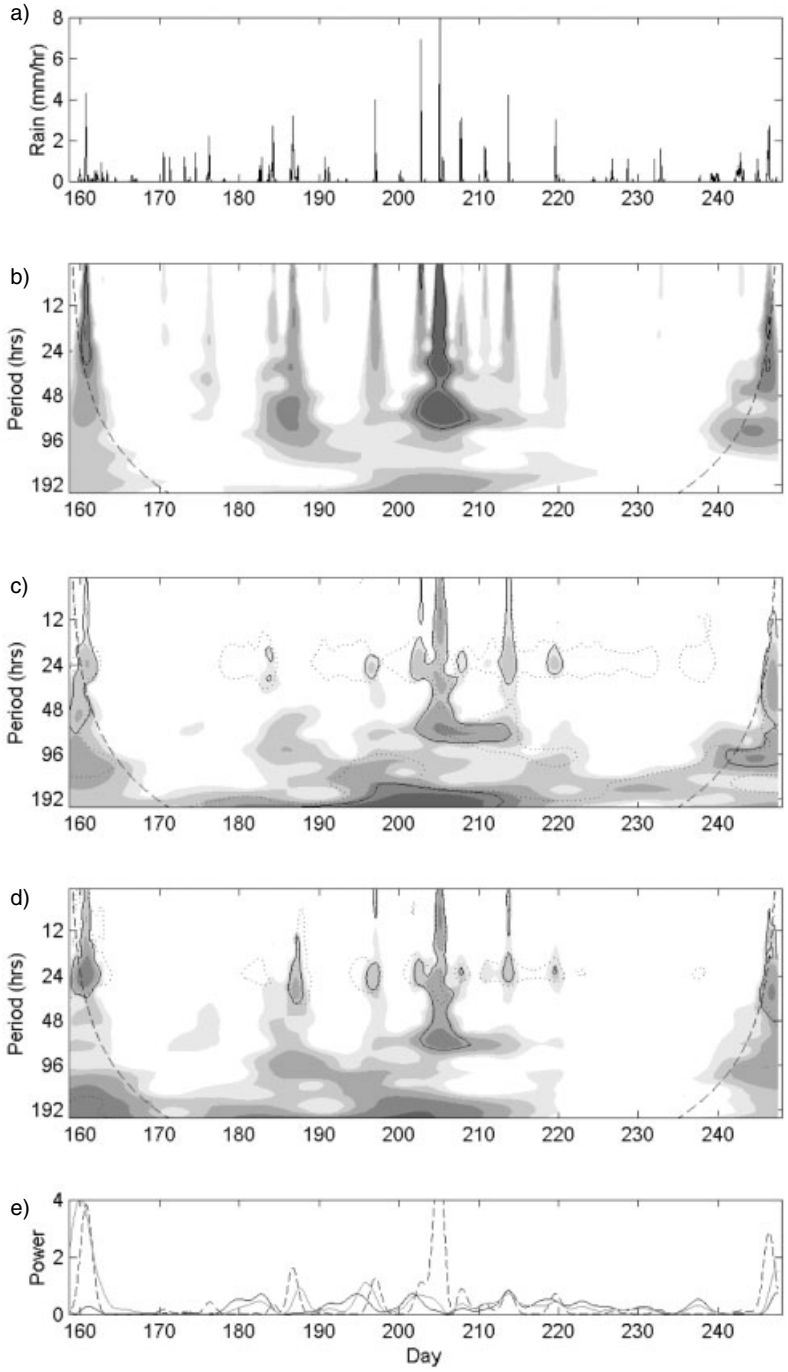

Figure 12. Wavelet analysis of hourly precipitation 2000: (a) hourly rain (mm); (b) $W_n^{PP}(s)$ contoured at variance 0·25, 0·5, 1, 2, and 4 (light to dark grey); (c) $W_n^{PQ_{GL}}(s)$; (d) $W_n^{PQ_{BR}}(s)$. The cross-wavelet spectrums are contoured at powers of 0·25, 0·5, 1·0, and 4·0. The black contour line is the 95% confidence level of the cross-spectrum, the dashed contour is the 95% confidence level of the local discharge spectrum, and the dashed black line on the edges is the COI. (e) $W_n^{PP}(24)$ (dashed), $W_n^{QQ}(24)$ for GL (black), and $W_n^{QQ}(24)$ BR (grey)

a recession of the discharge hydrograph. Therefore, in a snowmelt-fed catchment, the retreat of the snowpack should be indicated by a decrease in the wavelet power $W_n^{QQ}(s)$ at 24 h and low-frequency scales, and a drop in discharge below the seasonal mean (when the normalized discharge drops below zero). The loss of the snowpack as a storage reservoir might also be indicated by a decrease in the phase difference between the temperature and discharge signals at diurnal scales, since the travel time of meltwater to the stream should decrease. Since the exposure of glacier ice amplifies the response of discharge temperature variations, this event should be marked by a significant increase in the daily mean discharge, increases in the wavelet power at diurnal and longer time scales, and by an increase in the temperature–discharge cross-wavelet covariance for the glacial stream. The development of major channels in the glacier system may lead to further increases in the wavelet power for discharge at 24 h and shorter time scales, as well as decreases in the lag between diurnal temperature and discharge cycles, due to the faster transfer of meltwater and rainfall runoff from ice surfaces (Fountain, 1996).

Discharge response to rainfall is indicated by sudden changes in the temperature–discharge phase difference. It is also shown by the presence of significant power in the discharge wavelet spectra that is not associated with significant covariance in the temperature–discharge cross-spectra (this implies that the discharge variability is not due to temperature-induced meltwater runoff, but to a non-meltwater source such as rainfall). The type of precipitation is also important, as summer snowfalls may drastically reduce the melt response of old snow and glacier ice for periods of several days (Fountain, 1996).

Changes in the type of flow routing in a catchment, such as a switch from shallow subsurface flow to overland flow of meltwater due to the saturation of soils, are more difficult to identify using the wavelet analyses. However, a delay between the peak temperature–discharge covariance, or the precipitation–discharge covariance, and the peak in the wavelet power for discharge suggests that the meltwater or precipitation is being retained in the snow and/or soils before being routed to the stream (Figure 10b, days 160–164; Figure 12d, days 160–164, 186–188). On the other hand, the overland flow routing of rain or meltwater may be indicated by strong short-scale (6–12 h) wavelet power for discharge that coincides with a precipitation event (Figure 8b, day 167).

Interpretation and evaluation of the results

The inter-annual variations in air temperature and snowfall conditions at Bow Lake (Table II) can largely be explained by the 1998 El Niño event and the strong La Niña conditions that followed in 1999 and 2000. The southern oscillation index (SOI) anomaly for 1951–2000 (Figure 13) illustrates that 1997–98 was one of the strongest El Niño events on record, and 1999 and 2000 experienced relatively strong La Niña conditions. The west coast of Canada and the USA typically experience considerably warmer temperatures, lower snowfall, and lower stream flows in the year following the onset of El Niño (Kiladis and Diaz, 1989; Redmond and Koch, 1991; Kahya and Dracup, 1993; Brown, 1998). At Bow Lake, the low snowfall in 1997–98, combined with

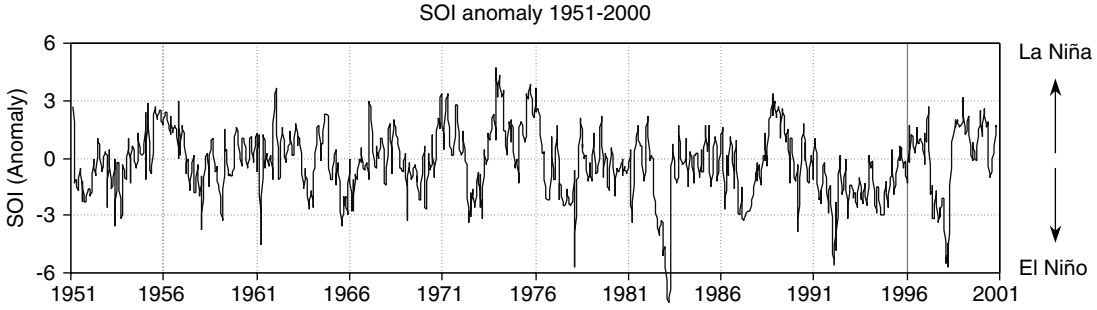

Figure 13. The SOI anomaly 1951–2000 (NOAA, 2000)

the high spring and summer temperatures in 1998, led to the early disappearance of snow from the catchments. This resulted in low seasonal discharge in the Bow River, but higher discharge in the glacial stream.

The results of the wavelet analyses highlight the unique hydrological regime brought on by the 1998 El Niño conditions. The early removal of snow from the catchments in 1998 is indicated by the fall of the normalized discharge in the Bow River below zero as early as day 195 (Table III). The low global wavelet power around the 120 h scale for the Bow River also illustrates that this stream was less responsive to weather-related melt forcing in 1998, as a result of the thin snowpack (Table III). The global power at the 12 and 24 h scales for the glacial stream was double the power at these scales in other years, probably as a result of the extensive exposure of glacial ice in 1998 (Table III). Table III also shows that the diurnal scale power for the Bow River and the glacial stream increased together for 1997, 1999, and 2000. In 1998, however, the 24 h power for the Bow River discharge was relatively low and the 24 h power for the glacial stream was at a maximum. The ratio of global 24 h power in the two streams (GL/BR) versus the diurnal-scale global power for the glacial stream ($\overline{W}_n^{QQ}(24)$ GL) also illustrates the dramatically different relationship between runoff in the two streams in 1998 (Table III). These results indicate that snowmelt was the dominant runoff source in the two streams in 1999 and 2000, and to a lesser extent in 1997. In 1998, the removal of snow from the catchments resulted in an exponential increase in the diurnal discharge response in the glacial stream due to significant ice melt, and a sharp reduction in response in the Bow River due to the complete and early removal of the snowpack.

The strong and persistent 12 h scale power in the glacial stream discharge wavelet spectrum during July and August 1998 (Figure 4b(ii), days 215–247) indicates that the exposure of glacial ice probably leads to the development of major channels within the glacial drainage system late in the summer. The persistence of the short-scale power in the glacial discharge signal strongly suggests that the signal is due primarily to an expansion of the drainage system as opposed to transient extreme floods from melt or precipitation (Rothlisberger and Lang, 1987). The shift in the phase lag from approximately 110° (7 h) to 70° (4·5 h) around day 190 in 1998 is also an indication of the exposure of glacial ice and/or the development of subglacial channels. The increase in the phase difference in the glacial stream around the same time that the 12 h discharge signal gained strength (Figure 8c, days 220–247) may seem to challenge this suggestion. However, there was a strong inverse relationship between the phase difference and the time of daily maximum air temperature for both streams during this period (Figure 14a), which indicates that the increase in lag was due to air temperatures peaking earlier in the day. Such a shift in the time of the daily air temperature peak was not observed at any other time in the 4 years of study. The air temperature for Bow Lake was estimated from the Bow Summit weather station for virtually all of this period (days 221–232, 234–247). Therefore, the increase in the phase difference at the end of the season in 1998 was most likely a result of a difference in the timing of the daily air temperature peaks at the two sites, rather than a change in runoff response. Figure 14b confirms that, between days 215 and 247, the time of peak discharge was generally constant.

In July and August 1997, there was an increase in the discharge and the 24 h power for the discharge wavelet spectra for the glacial stream. However, the power at the 24 h scale was much weaker than in 1998, and there was no evidence of any variability in discharge at lower scales (Figure 3a(i) and (ii)). This suggests that some ice was exposed on the glacier in that year, but that the degree of exposure was not nearly as extensive as in 1998, and that there was little development of the subglacial drainage system. Compared with 1999 and 2000, the low phase difference between air temperature and stream discharge in 1998 and 1997 (Table IV) indicates that the snowpack was more effective at retarding the runoff of the diurnal meltwater pulse in 1999 and 2000. In 1997 and 1998, the diurnal-scale variability in the Bow River discharge was maintained throughout most of the summer, with a temporal distribution of power very similar to that in the glacial wavelet spectra (Figures 3 and 4). This persistent diurnal cycle in the Bow River catchment indicates a continuing input of melt runoff from the small area of ice cover in the catchment in these years. This ice melt source only appears to have contributed significantly to Bow River runoff in years when the previous winter's snowpack was thin and/or summer temperatures were high (Table II). In 1999 and 2000, variability in the Bow River discharge at the 24 h scale was very low or absent through most of July and August, when the diurnal runoff signal gained strength in the glacial stream (Figures 5 and 6).

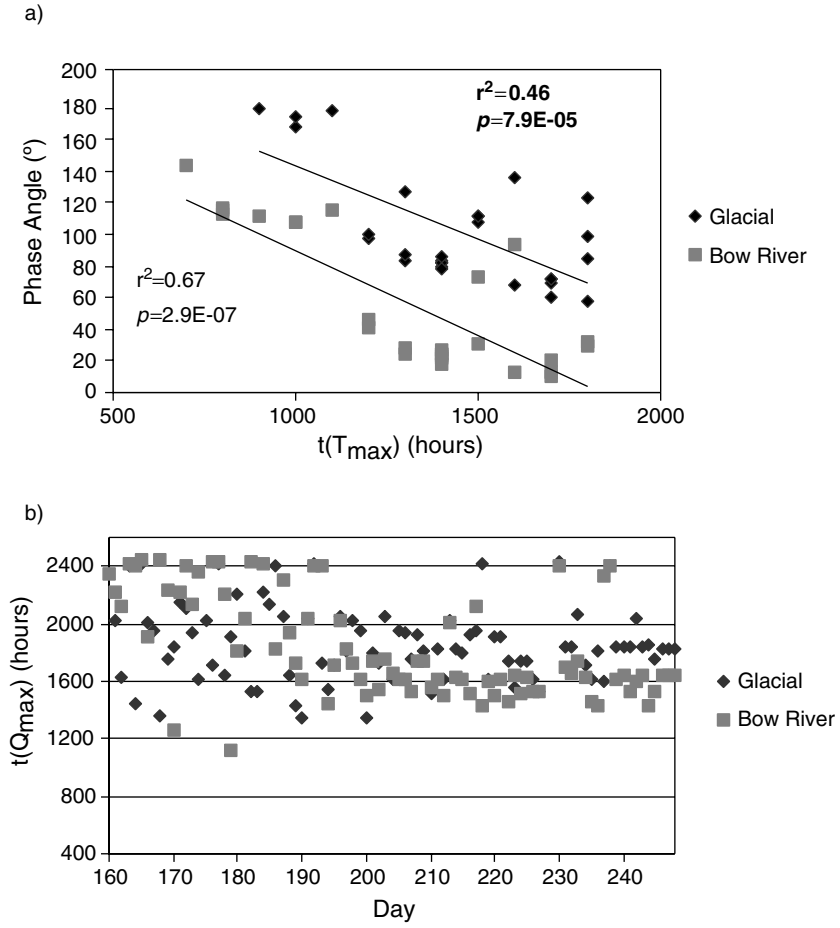

Figure 14. (a) The relationship between time of daily maximum air temperature $t(T_{\max})$ and the phase difference $\theta_n^{TQ}(24)$ at 12 : 00 for the glacial stream and the Bow River between days 215 and 247, 1998. The regression statistics were calculated after removal of outliers. (b) Time of daily maximum discharge $t(Q_{\max})$) for glacial and Bow River streams, 1998

The frequent significant variability in discharge at the lower scales (<24 h) and the rapid changes in discharge–temperature phase difference for the Bow River suggest that precipitation is a more important component of runoff and follows more direct flow routes in the Bow River catchment than in the glacial catchment. For example, between days 160 and 205, 2000, the phase difference for the Bow River showed several short-lived dramatic shifts. The glacial stream lags changed at approximately the same time as those for the Bow River, but the shifts were less pronounced in the glacial stream (Figure 10c). For the Bow River, there were also several instances of strong discharge wavelet power that were unrelated to strong temperature–discharge covariance. However, no such instances were observed for the glacial stream (Figure 10a and b, days 160–205). The covariance between precipitation and discharge was also much stronger for the Bow River than for the glacial stream at the beginning of the season (Figure 12). After day 205, however, the response of discharge to precipitation was higher for the glacial stream (Figure 12c and d). This implies that ice may have been exposed on the glacier or that soils in the Bow River catchment had a reduced moisture content and greater storage capacity, or both.

The retardation of snowmelt routing, as indicated by the mean annual phase difference between temperature and stream discharge, generally varied with the thickness of the seasonal snow pack and the size of the

catchment. Except in 1999, the phase lags were higher for the glacial stream than for the Bow River, and they were lowest in both streams in 1998 (Table IV).

By locating and quantifying the strength and significance of the variability in stream runoff at different scales, and the relationship between temperature and runoff cycles, the wavelet analyses appear to be a useful tool for comparing the relative contributions of water sources to runoff both seasonally and inter-annually. However, the wavelet analyses do not unambiguously identify changes in hydrological flow routing within the catchments. The phase difference between temperature and discharge is an indication of the relative influence of the snowpack on storage of meltwater, and strong wavelet power at very short time scales (6–12 h) can indicate the influence of faster flow routes, either within the glacial drainage system or from overland flow. However, it was anticipated that the wavelet analyses might help differentiate between periods of overland flow and shallow subsurface flow during the snowmelt period. Such changes are, however, no more obvious in the wavelet results than they are in the discharge hydrographs.

CONCLUSIONS

Wavelet analysis is a fast and effective tool to quantify and compare the inter-annual variability in runoff and the relationships between runoff and temperature/rainfall in glacial and nival catchments, especially when dealing with large data sets. The strong power at 12 h and diurnal scales in the local wavelet spectra for glacial runoff in 1998 indicates that significant ice exposure and the development of channelized glacial drainage occurred in 1998. This was due to the low snowfall and high temperatures experienced at Bow Lake during the 1997–98 El Niño event. The analyses showed that the early retreat of the snowpack, as observed in 1997 and 1998, led to a continuing input of melt runoff from a small area of ice cover in the Bow River catchment. Rainfall had a stronger influence on runoff, and followed quicker flow paths in the Bow River catchment than in the glacial catchment. The results also illustrate that the snowpack thickness and catchment size were the primary controls on the phase difference between diurnal temperature and discharge cycles.

By quantifying the strength and statistical significance of variance in discharge, and of the covariance between discharge and temperature/precipitation forcing, at different scales of response, wavelet analysis appears to be a useful tool for identifying inter-annual and seasonal changes in the relative contributions of different water sources to runoff. Wavelet analyses can also identify general changes in the flow routing time of snow- and ice-melt through the catchment, but they are largely incapable of identifying changes or differences in the nature of the flow routing (e.g. overland flow versus through flow) between or within a catchment.

ACKNOWLEDGEMENTS

NSERC Strategic Grant #192943–96 provided funding to D.W. Schindler and M. Sharp, and NSERC PGS scholarships to M.J. Lafrenière. Additional funding was provided by the Geological Society of America and a Canadian Circumpolar Institute Boreal Alberta Research Grant. We are grateful to Parks Canada for permission to conduct field research in Banff National Park. Snowpack and temperature data for Bow Summit were provided by Alberta Environment. Thanks to Jules Blais, Serge Larocque, Tobias Herman, Brad Thomas, Shawna Bassani-Moore, Mark Skidmore, Anthony Arendt, Joel Barker, Candice Stuart, Luke Copland, Trudy Wohlleben, Nigel Atkinson, and Karen Heppenstall for their assistance in installation, removal and maintenance of the weather and gauging stations.

REFERENCES

Blais JM, Schindler DW, Muir DCG, Donald D, Sharp MJ, Lafrenière MJ, Braekevelt E, Strachan W, Comba M, Backus S. 2001a. Melting glaciers dominate sources of persistent organochlorines to subalpine Bow Lake in Banff National Park, Canada. *Ambio* **30**(7): 410–415.

Blais JM, Schindler DW, Sharp M, Braekevelt E, Lafrenière M, McDonald K, Muir DCG, Strachan W. 2001b. Fluxes of semivolatile organochlorine compounds in Bow Lake, a high altitude, glacier-fed, subalpine lake in the Canadian Rocky Mountains. *Limnology and Oceanography* **46**(8): 2019–2031.

Boyer EW, Hornberger GM, Bencala KE, McKnight DM. 1997. Response characteristics of DOC flushing in an alpine catchment. *Hydrological Processes* **11**: 1635–1647.

Braithwaite R. 1981. On glacier energy balance, ablation, and air temperature. *Journal of Glaciology* **27**(97): 381–391.

Brooks PD, Williams MW, Schmidt SK. 1995. Snowpack controls on soil nitrogen dynamics in the Colorado alpine. In *Biogeochemistry of Seasonally Snow-Covered Catchments*, Tonnessen KA, Williams MW, Tranter M (eds). IAHS Publication no. 228. IAHS: Wallingford; 283–302.

Brown R. 1998. El Niño and North American snow cover. In *Proceedings of 55th Eastern Snow Conference*, Jackson NH; 1–13. www1.tor.ec.gc.ca/crysys/brown98/ESC98Paper.html.

Daubechies I. 1990. The wavelet transform time–frequency localization and signal analysis. *IEEE Transactions or Information Theory* **36**: 961–1004.

Daubechies I. 1992. *Ten Lectures on Wavelets*. Society for Industrial and Applied Mathematics: Philadelphia.

Dingman LS. 1993. Stream-gauging methods for short-term studies. In *Physical Hydrology*. Prentice-Hall: Englewood Cliffs, NJ; 536–552.

Dracup JA, Kahya E. 1994. The relationship between U.S. streamflow and La Niña events. *Water Resources Research* **30**(7): 2133–2141.

Fountain AG. 1996. Effect of snow and firn hydrology on the physical and chemical characteristics of glacial runoff. *Hydrological Processes* **10**: 509–521.

Gudmundsson G. 1970. Short term variations of a glacier-fed river. *Tellus* **22**: 341–353.

Gudmundsson G, Sigbjarnarson G. 1972. Analysis of glacier run-off and meteorological observations. *Journal of Glaciology* **11**(63): 303–318.

Gurnell AM, Clark MJ, Hill CT. 1992. Analysis and interpretation of patterns within and between hydroclimatological time series in an alpine glacier basin. *Earth Surface Processes and Landforms* **17**: 821–839.

Hodgkins R. 2001. Seasonal evolution of meltwater generation, storage and discharge at a non-temperate glacier in Svalbard. *Hydrological Processes* **15**(3): 441–460.

Kadambe S, Boudreaux-Bartels GF. 1992. Application of the wavelet transform for pitched detection of speech signals. *IEEE Transactions or Information Theory* **38**: 917–924.

Kahya E, Dracup JA. 1993. U.S. streamflow patterns in relation to the El Niño/southern oscillation. *Water Resources Research* **29**(8): 2491–2503.

Kiladis GN, Diaz HF. 1989. Global climatic anomalies associated with extremes in the southern oscillation. *Journal of Climate* **2**: 1069–1090.

Kronland-Martinet R, Morlet J, Grossman A. 1987. The analysis of sound patterns through wavelet transforms. *International Journal of Pattern Recognition and Artificial Intelligence* **1**: 97–126.

Labat D, Ababou R, Mangin A. 2000. Rainfall-runoff relations for karstic springs. Part II: continuous wavelet and discrete orthogonal multiresolution analyses. *Journal of Hydrology* **238**: 149–178.

Misiti M, Misiti Y, Oppenheim G, Poggi J-M. 1996. *Wavelet Toolbox User's Guide (for use with MATLAB)*. The Math Works Inc.: Natwick, MA.

Moore RD, Demuth MN. 2001. Mass balance and streamflow variability at Place Glacier, Canada, in relation to recent climate fluctuations. *Hydrological Processes* **15**(18): 3473–3486.

NOAA. 2000. *Southern oscillation index (SOI): (Stand Tahiti–Stand Darwin) sea level pressure*. ftp://ftp.ncep.noaa.gov/pub/cpc/wd52dg/data/indices/soi [last accessed 26 June 2001].

Redmond KT, Koch RW. 1991. Surface climate and streamflow variability in the western United States and their relationship to large-scale circulation indices. *Water Resources Research* **27**(9): 2381–2399.

Richards K, Sharp MJ, Arnold N, Gurnell A, Clark M, Tranter M, Nienow P, Brown G, Willis I, Lawson W. 1996. An integrated approach to modelling hydrology and water quality in glacierized catchments. *Hydrological Processes* **10**: 479–508.

Rothlisberger H, Lang H. 1987. Glacial hydrology. In *Glacio-Fluvial Sediment Transfer: An Alpine Perspective*, Gurnell A, Clark MJ (eds). John Wiley & Sons: Chichester; 207–284.

Schiff S. 1992. Resolving time-series structure with a controlled wavelet transform. *Optical Engineering* **31**(1): 2492–2495.

Smith L, Turcotte DL, Isacks BL. 1998. Stream flow characterization and feature detection using a discrete wavelet transform. *Hydrological Processes* **12**: 233–249.

Stoddard JL. 1995. Episodic acidification during snowmelt of high elevation lakes in the Sierra Nevada Mountains of California. *Water, Soil, and Air Pollution* **85**: 353–358.

Torrence C, Compo GP. 1998. A practical guide to wavelet analysis. *Bulletin of the American Meteorological Society* **79**(1): 62–78.

Whitfield PH, Dohan K. 1997. Identification and characterization of water quality transients using wavelet analysis II. Application to electronic water quality data. *Water Science and Technology* **36**(5): 337–348.

